

January 13, 2020

The Proper Motion of Sagittarius A*: III. The Case for a Supermassive Black Hole

M. J. Reid

Center for Astrophysics | Harvard & Smithsonian, Cambridge, MA 02138

reid@cfa.harvard.edu

A. Brunthaler

Max-Planck-Institut für Radioastronomie, Auf dem Hügel 69, D-53121 Bonn, Germany

brunthal@mpifr-bonn.mpg.de

ABSTRACT

We report measurements with the Very Long Baseline Array of the proper motion of Sgr A* relative to two extragalactic radio sources spanning 18 years. The apparent motion of Sgr A* is -6.411 ± 0.008 mas y^{-1} along the Galactic plane and -0.219 ± 0.007 mas y^{-1} toward the North Galactic Pole. This apparent motion can almost entirely be attributed to the effects of the Sun’s orbit about the Galactic center. Removing these effects yields residuals of -0.58 ± 2.23 km s^{-1} in the direction of Galactic rotation and -0.85 ± 0.75 km s^{-1} toward the North Galactic Pole. A maximum-likelihood analysis of the motion, both in the Galactic plane and perpendicular to it, expected for a massive object within the Galactic center stellar cluster indicates that the radiative source, Sgr A*, contains more than about 25% of the gravitational mass of $4 \times 10^6 M_{\odot}$ deduced from stellar orbits. The intrinsic size of Sgr A* is comparable to its Schwarzschild radius, and the implied mass density of $\gtrsim 4 \times 10^{23} M_{\odot} \text{ pc}^{-3}$ is very close to that expected for a black hole, providing overwhelming evidence that it is indeed a super-massive black hole. Finally, the existence of “intermediate mass” black holes more massive than $\approx 3 \times 10^4 M_{\odot}$ between approximately 0.003 and 0.1 pc from Sgr A* are excluded.

Subject headings: Individual Sources: Sgr A*; Black Holes; Galaxy: Center, Fundamental Parameters, Structure; Astrometry

1. Introduction

At the Galactic center, stars orbit an unseen mass of $4 \times 10^6 M_\odot$ (eg, Boehle et al. 2016; Gillessen et al. 2017), and the compact radio source Sgr A* projects to within ≈ 1 mas (≈ 8 AU) of the gravitational focal position (Menten et al. 1997; Reid et al. 2007) of these stars. If we are to conclude that the Galactic center harbors a supermassive black hole, a critical question is how much of the unseen mass can be directly tied to Sgr A*. Since the luminosity of Sgr A* is only comparable to a stellar source, other information is needed to establish if it is a supermassive black hole. To that end, we have been measuring the position of Sgr A* with the National Radio Astronomy Observatory’s¹ Very Long Baseline Array (VLBA) since 1995, since a very massive object at the dynamical center of the Galaxy should be nearly motionless.

The apparent motion of Sgr A*, relative to extragalactic radio sources, contains the reflex of the Sun’s velocity in its orbit about the Galactic center, plus any intrinsic motion of Sgr A* itself. In Reid et al. (1999) and Reid & Brunthaler (2004), hereafter Papers I and II, we published results from the first 8 years of observation. We showed that the component of the apparent motion of Sgr A* *perpendicular* to the Galactic plane could be explained by the motion of the Sun toward the North Galactic Pole, limiting the intrinsic motion of Sgr A* to $\lesssim 1 \text{ km s}^{-1}$ in one dimension. Since a massive object embedded in a dense stellar cluster suffers gravitational Brownian motion and reaches thermal equilibrium with the perturbing stars (Chatterjee, Hernquist, & Loeb 2002), the observed lack of motion for Sgr A* provided a lower limit of $\sim 0.4 \times 10^6 M_\odot$ for Sgr A* (Reid & Brunthaler 2004). This clearly associated a very large mass with the radiative source Sgr A*, and greatly strengthened the already strong case for Sgr A* being a super-massive black hole (SMBH).

In this paper, we report new observations which now span 18 years, reducing proper motion uncertainties by a factor of three to less than $\pm 10 \mu\text{as yr}^{-1}$, both in and out of the Galactic plane. Coupling these results with independent measurements of the angular motion of the Sun in its orbit about the Galactic center, we are now able to use two dimensions of velocity information to provide a stronger and more robust lower limit for the mass of Sgr A*, significantly increasing confidence that it is indeed a black hole.

¹The National Radio Astronomy Observatory is operated by Associated Universities Inc., under a cooperative agreement with the National Science Foundation.

2. Observations and Results

Our observations using the National Radio Astronomy Observatory’s VLBA started in 1995 and have now continued to 2013. Paper I reported early results for observations from 1995 through 1997, and observations through 2003 were reported in Paper II. Here we present new observations conducted in 2007 and 2013 under VLBA programs BR124 and BR173. As VLBI technology progressed we increased the recorded data rates. For BR124 we observed with eight 8-MHz bands with Nyquist sampling and 2-bits per sample for a total sampling rate of 256 Mb s^{-1} . The observations spanned 8 hours and we placed three geodetic-like blocks at the beginning, middle and end of the tracks in order to measure and remove tropospheric and clock delays. We switched between sources every 15 seconds, using Sgr A* as the phase-reference for the background sources. For BR173 we observed with 16 32-MHz bands with Nyquist sampling and 2 bits-per-sample for a total sampling rate of 2 Gb s^{-1} . These observations spanned 6 hours and we placed four geodetic-like blocks evenly spaced throughout the observations, and we switched between sources every 17 seconds. Details of the calibration procedures can be found in Papers I and II.

After calibration, we imaged all sources and measured their positions by fitting elliptical Gaussian brightness distributions. Table 1 lists all of our position measurements of Sgr A* relative to two compact extragalactic radio sources, J1745–2820 and J1748–2907, in J2000 Equatorial and also Galactic coordinates. The measurements were made at the highest astrometrically useful frequency of the VLBA of 43 GHz in order to minimize the effects of strong interstellar scattering toward the Galactic center.² Position uncertainties include estimates of systematic effects, dominated by small residual errors in modeling atmospheric delays.

2.1. Proper Motion of Sgr A*

The positions on the sky of Sgr A*, relative to the two background sources, are plotted in Fig. 1. The observations now span 18 years and the linear trends reported in Papers I and II continue. Variance-weighted least-squares fits to the position versus time of Sgr A* relative to J1745–2820 and J1748–2907 are given in Table 2 and plotted with dashed lines in Fig. 1. The results for the two background sources are consistent and differencing the motions

² While some antennas of the VLBA have 86 GHz receivers, the system sensitivity is approximately a factor of five poorer than at 43 GHz. In addition, interferometer coherence times are a factor of two shorter at 86 GHz compared to 43 GHz. These factors strongly favor 43 GHz observations requiring phase-referencing needed for astrometry.

with respect to the background sources shows no significant motion. Assuming that the background sources are sufficiently distant that they have negligible intrinsic angular motion, we average the two results and estimate Sgr A*'s apparent motion to be -3.156 ± 0.006 and -5.585 ± 0.010 mas yr $^{-1}$ in the easterly and northerly directions, respectively.

We re-fitted for motions in Galactic coordinates (see Table 2), yielding apparent motion components for Sgr A* in Galactic longitude of -6.411 ± 0.008 mas yr $^{-1}$ and in latitude of -0.219 ± 0.007 mas yr $^{-1}$. The data and fits are displayed in Fig. 2. Adopting a distance to the Galactic center of $R_0 = 8.15$ kpc (Gravity Collaboration et al. 2019; Do et al. 2019; Reid et al. 2019), Sgr A* *appears* to be moving predominantly along the Galactic plane with a tangential (toward increasing longitude) speed of -247.69 ± 0.33 km s $^{-1}$ and toward the North Galactic Pole with a speed of -8.45 ± 0.26 km s $^{-1}$.

2.2. Acceleration of Sgr A*

We also investigated the possibility that Sgr A* is being accelerated by, for example, an intermediate mass black hole (IMBH). When we added an acceleration parameter in the motion fits, we obtain easterly and northerly acceleration estimates of -0.0026 ± 0.0030 mas yr $^{-2}$ and -0.0050 ± 0.0038 mas yr $^{-2}$ relative to J1745–2820 and 0.0058 ± 0.0029 mas yr $^{-2}$ and 0.0129 ± 0.0074 mas yr $^{-2}$ relative to J1748–2907. A variance-weighted average of the two acceleration results gives easterly and northerly motions of 0.0017 ± 0.0021 mas yr $^{-2}$ and -0.0013 ± 0.0034 mas yr $^{-2}$. These acceleration estimates are an order of magnitude improvement over our results in Paper II. They are consistent with no measurable acceleration, with a 2σ upper limit of 0.0080 mas yr $^{-2}$ (0.31 km s $^{-1}$ yr $^{-1}$) for the magnitude of the two-dimensional acceleration vector. Acceleration limits are potentially interesting as they require no correction for Solar orbital acceleration, which is $\sim 10^{-7}$ mas yr $^{-2}$ (Gould & Ramírez 1998).

Interestingly, the stellar cluster IRS 13E has marginal evidence for an IMBH of 3×10^4 M_\odot (eg, Genzel, Eisenhauer & Gillessen 2010). The cluster projects within ≈ 3 asec of Sgr A*, corresponding to a linear offset of ≈ 0.1 pc. Assuming its three-dimensional distance from Sgr A* is comparable to this offset, such an IMBH would likely induce an acceleration of 0.4 km s $^{-1}$ yr $^{-1}$ and a linear motion of about 3 km s $^{-1}$ for Sgr A*. Fig. 3 presents the regions of IMBH mass and radius from Sgr A* that are allowed for and excluded by the current observations. Our limits make an IMBH of $\approx 3 \times 10^4$ M_\odot between 0.003 and 0.1 pc from Sgr A* unlikely and strongly exclude a more massive object of $\gtrsim 10^5$ M_\odot , as does dynamical modeling of the orbit of star S02 (S2) by Naoz et al. (2019). Note that a modest increase in the time span of our astrometric observations could better test the

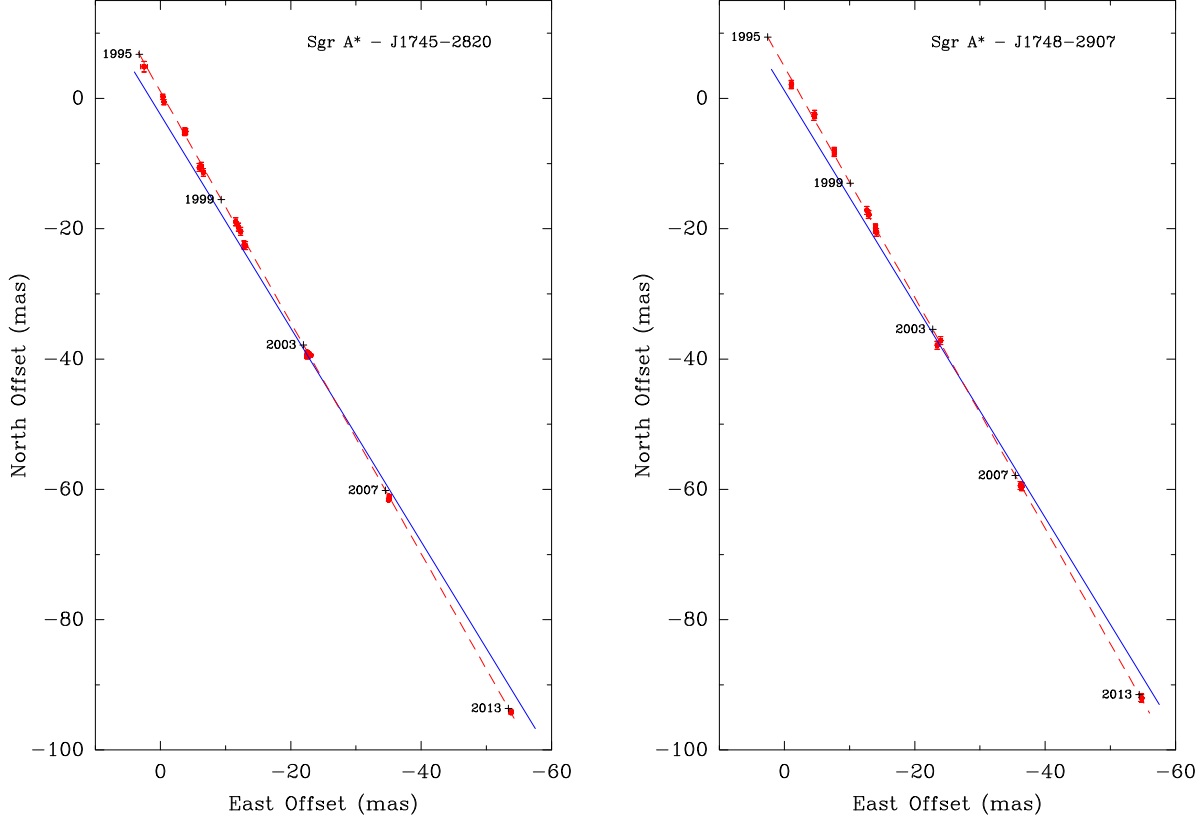


Fig. 1.— Position residuals of Sgr A* relative to J1745–2820 (left panel) and J1748–2907 (right panel) on the plane of the sky. Measurements are indicated with ellipses, whose sizes are the scatter-broadened image of Sgr A* at 43 GHz, and 1σ error bars which are dominated by systematic uncertainties. The dashed lines are least-squares fitted proper motions; the solid line gives the orientation of the Galactic plane when looking toward the Galactic center.

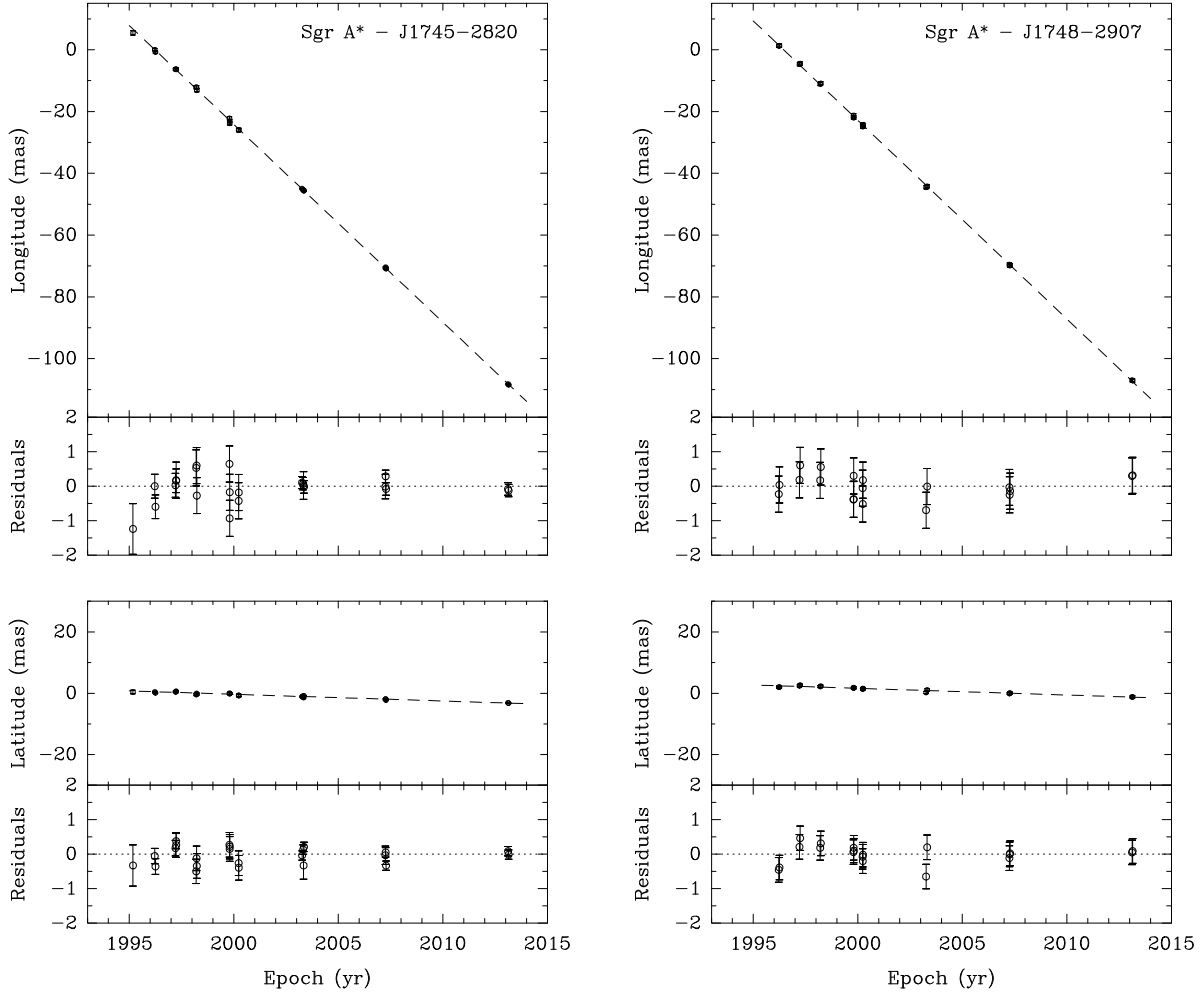


Fig. 2.— Galactic longitude and latitude vs time for Sgr A* relative to J1745–2820 (left panels) and J1748–2907 (right panels). Dashed lines are variance-weighted least-squares fits to the data, and the residuals to those fits are shown below each plot.

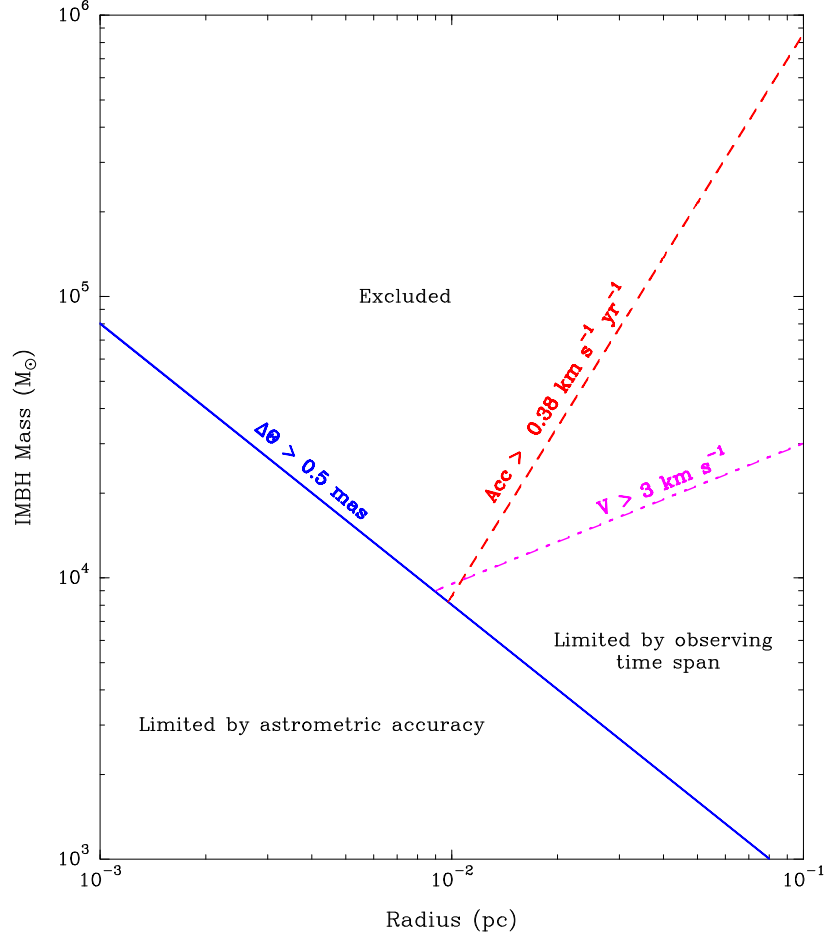


Fig. 3.— Limits on the mass of an intermediate mass black hole (IMBH) orbiting a $4 \times 10^6 M_{\odot}$ Sgr A* as a function of orbital radius. The blue line divides the parameter space for angular excursion of Sgr A* of 0.5 mas, below which it could appear as jitter within our current astrometric accuracy. The dashed red line corresponds to our upper limit on the (2-D) magnitude of the acceleration of Sgr A*, and the dot-dashed magenta line corresponds to similar limits on the velocity of Sgr A*. The region excluded by these constraints is above the dashed lines, which could be improved by a longer time span of observations.

IMBH’s existence, since for uniform sampling acceleration accuracy improves as the $5/2$ power and motion accuracy improves as the $3/2$ power of time spanned.

3. Limits on the Mass of Sgr A*

Some of the so-called “S” stars have been seen projected within ~ 0.001 pc of Sgr A* and move at thousands of km s^{-1} (Schödel et al. 2002; Ghez et al. 2005) as they orbit a dark mass concentration. In contrast, Sgr A*, which is located within 0.00004 pc of the gravitation focus of the orbiting stars (Menten et al. 1997; Reid et al. 2003; Reid et al. 2007), has an intrinsic motion (relative to distant quasars) of less than a few km s^{-1} , strongly suggesting that it is very massive. For example, were Sgr A* only a $10 M_{\odot}$ black hole in an X-ray binary, which would be consistent with its meager luminosity, it too should be moving at a great speed. However, a massive object in the presence of large numbers of stars experiences gravitational Brownian motion, which is expected to result in equipartition of kinetic energy between the massive object and individual stars (Chatterjee, Hernquist, & Loeb 2002; Dorband, Hemsendorf & Merritt 2003; Merritt, Berczik & Laun 2007). In Paper II, we performed detailed simulations of the motion of a massive object orbited by $\sim 10^6 - 10^7$ stars within its sphere of influence. These simulations confirmed that equipartition of kinetic energy is indeed achieved, and that a $4 \times 10^6 M_{\odot}$ object would be expected to have a (one-dimensional) motion of between 0.18 and 0.30 km s^{-1} , depending on the nature of the stellar mass function. In addition, a cluster of dark stellar remnants summing to $0.4 \times 10^6 M_{\odot}$ could contribute an additional 0.2 km s^{-1} to the motion of the massive object. In this context, an upper limit to Sgr A*’s intrinsic motion can provide a lower limit to its mass.

Compared to Paper II, our latest results for the apparent motion of Sgr A* have decreased the motion uncertainties by a factor of three. Also, in Paper II we used only the component of motion of Sgr A* perpendicular to the Galactic plane, corrected for the Sun’s motion, to provide a lower limit for the mass of Sgr A*. The motion of Sgr A* in the Galactic plane was not used since, at the time, the correction for the orbital motion of the Sun was quite uncertain ($\pm 20 \text{ km s}^{-1}$). The Sun’s motion in its Galactic orbit is now known to much higher accuracy, and we can now use the Galactic longitude motion to complement the latitude motion in order to more tightly and robustly constrain the mass of Sgr A*.

By modeling parallaxes and proper motions of about 150 massive young stars with maser emission, Reid et al. (2019) estimate the angular speed of the Sun in its Galactic orbit with sub-percent accuracy: $(\Theta_0 + V_{\odot})/R_0 = 30.32 \pm 0.27 \text{ km s}^{-1} \text{ kpc}^{-1}$, where Θ_0 is the circular orbital speed in the Galaxy at the Sun and V_{\odot} accounts for the Sun’s deviation from a perfect circular orbit. In Table 3, we detail the values used to remove the effects of

the Sun’s motion, in order to estimate the intrinsic motion of Sgr A*, both in and out of the Galactic plane. We find that Sgr A* is nearly motionless with longitude and latitude speeds of -0.58 ± 2.23 and -0.85 ± 0.75 km s⁻¹, respectively. Since these speeds came from differencing independently determined angular motions, the adopted value of R_0 of 8.15 kpc used to convert the differences to linear motions appears only as a final scale factor, and since R_0 is now known to better than 2% accuracy (Gravity Collaboration et al. 2019; Do et al. 2019; Reid et al. 2019), its uncertainty is not important for our application.

In order to estimate how massive is Sgr A*, we simulate the effects of the central star cluster on a massive central object. Using the same approach as in Paper II, we generate 10^3 random configurations of stars orbiting an object with a given trial mass, follow the system for the time spanned by our observations (now 18 years), and infer the motion of the trial object from the change in center of mass of the orbiting stars. We compare the simulated components of motion in each of two dimensions with trials drawn from Gaussian distributions, which are consistent with our observed intrinsic motion of Sgr A* in Galactic longitude and latitude. We keep track of the fraction of trials that give at least one component of the massive object’s velocity which is inconsistent with our observed limits. We then repeat the simulation with different trial masses in order to trace the distribution as a function of mass. In contrast to Paper II, which only used the latitude motion of Sgr A* to compare to the simulations, we now use two components (latitude and longitude) to better constrain Sgr A*’s mass. This significantly improves both the lower limit on the mass of Sgr A* and the robustness of the mass estimate.

In Paper II we evaluated three stellar initial mass functions (IMFs): a standard IMF, a top-heavy IMF with a high-mass index by flatter by 0.5, and one flatter by 1.0. Given strong evidence for a top-heavy IMF in the Galactic center region, but an uncertain flattening at high masses (eg, Figer et al. 1999; Stolte, Grebel, Brandner, & Figer 2002; Genzel, Eisenhauer & Gillessen 2010), we conservatively adopt the moderately flattened IMFs considered in Paper II (with an index flatter by 0.5). We assume the broken power-law radial distribution of stars given by Eq. 4 of Genzel, Eisenhauer & Gillessen (2010). Specifically, our fiducial model has a volume density of stars given by $\rho_*(R) = 1.35 \times 10^6 (R/0.25\text{pc})^{-\gamma} \text{M}_\odot\text{kpc}^{-3}$, with $\gamma = 1.3$ and 1.8 inside and outside of $R = 0.25$ pc, respectively. We then generate random orbital parameters with semi-major axes between $R = 100$ AU (approximately the smallest radius observed for stars) and 2.9 pc (corresponding to the radius of the sphere of influence of a $4 \times 10^6 \text{M}_\odot$ central mass in the Galactic center).

In Fig. 4 we plot the results of these simulations with a solid blue line. We find that half of the trials would be detected were Sgr A* less massive than $0.8 \times 10^6 \text{M}_\odot$, a factor of two stronger limit than in Paper II. Importantly, our result for 95% confidence (i.e., 5%

undetected) is now $0.2 \times 10^6 M_\odot$, a factor of 200 improvement over the result in Paper II. This improvement comes mostly from the use of two dimensions of motion, compared to the one dimension available in Paper II. For comparison, we repeated the simulations using the stellar cluster model employed in Paper II and plot the results with a red dash-dotted line in Fig. 4. The differences between the stellar cluster models results only in small differences in the final results.

Since one expects a significant population of stellar remnants to accumulate in the Galactic center, we added a population of stellar-mass black holes to the fiducial model of the central cluster and re-ran the simulations. Following the models of Freitag, Amaro-Seoane & Kalogera (2006), we added a total mass of $7 \times 10^4 M_\odot$ in black holes between radii of 100 AU and 0.2 pc. This corresponds to less than 2% of the mass within 0.2 pc of the center. We assumed a flat distribution in mass between 6 and $30 M_\odot$, which results in about 4,000 black holes, and a cusp-like radial distribution with a Bahcall-Wolff power-law index of $-7/4$. The results of these simulations are shown with the black dashed line in Fig. 4. As expected, the motions of Sgr A* increase, but only modestly, and 50% of the trials would be detected were Sgr A* to hold $1.0 \times 10^6 M_\odot$.

Note that all of our simulations use smooth distributions of stars, without any clumping. Since clumping would increase the simulated motion of Sgr A*, our mass limits are very conservative. Thus, we adopt a round-number mass of $1.0 \times 10^6 M_\odot$ as a maximum-likelihood lower limit for the mass of the radiative source, Sgr A*, when we explore its significance in the next section.

4. Is Sgr A* a Super-Massive Black Hole

Given that the radiative source Sgr A* likely has a mass greater than $10^6 M_\odot$, how does this help answer the question “is it a black hole”? If one can show that sufficient mass is contained within a small enough volume, Einstein’s theory of General Relativity requires a black hole. This leads to a maximum mass density that matter can achieve before a black hole forms. Thus, the case for the existence of supermassive black holes centers on observations of objects that approach a critical mass density. The size of a black hole of a given mass can be defined by its Schwarzschild radius, $R_{Sch} = 2GM/c^2$, where G is the gravitational constant, M the mass of the black hole, and c is the speed of light. However, any matter that comes within $3R_{Sch}$ of a (non-rotating) hole cannot achieve a stable orbit and falls directly into the black hole. Thus, a critical mass density, ρ_{crit} , to require a black

hole is the mass divided by the volume enclosed by $3R_{Sch}$:

$$\rho_{crit} = \frac{M}{(4\pi/3)(3R_{Sch})^3} \quad .$$

Substituting the relation for R_{Sch} , we find

$$\rho_{crit} = \frac{c^6}{288\pi G^3 M^2} \quad .$$

Note that this density depends inversely as the square of the mass.³

An alternative “linear” density, ϕ_{crit} , defined as $M/3R_{Sch}$ provides a simple mass-independent parameter that can be used to establish a black hole:

$$\phi_{crit} = \frac{2G}{3c^2} \quad .$$

Table 4 lists critical linear and volume density limits as established from various observations and updated from Reid (2009). The first table entry is for globular clusters, which can have upwards of $\sim 10^6$ stars within a radius of ~ 1 pc. This provides a reference point for relatively high stellar densities that are commonly achieved in galaxies. The last table entry gives the critical linear and volume densities for a theoretical SMBH of $4 \times 10^6 M_\odot$ assuming a radius of $3R_{Sch}$. If one can show that these critical densities are achieved, the case for a supermassive black hole is established with near certainty.

Now we consider systems only with enclosed mass estimates from well-defined Keplerian orbits. The second entry in Table 4 is based on observations of water masers in the center of the galaxy NGC 4258. Very Long Baseline Interferometric (VLBI) observations with angular resolution of 0.4 mas show that these masers originate from a slightly warped, thin disk of gas within an angular radius of about 3 mas (2×10^4 AU at the distance of the galaxy). The observed rotational speeds of 900 km s^{-1} are consistent with Keplerian orbits about a central mass of $4 \times 10^7 M_\odot$. The implied volume density is nearly five orders of magnitude above stellar densities in globular clusters, effectively ruling out a cluster of normal stars⁴.

³ Interestingly, the critical density reaches that of water for a 30-million solar mass black hole, 10^{15} times lower than for a 1 solar mass black hole. Thus, for example, an “ocean” contained within the orbit of Mars would be a black hole.

⁴These observations, and those for dozens of other galaxies, certainly provide strong evidence that supermassive black holes are found at the centers of active galaxies. Were one to place $\sim 10^7$ stars inside a radius of ~ 0.1 pc, the system would be dynamically unstable. Less massive stars would be expelled while dynamical friction would cause massive stars to sink to the center where they could possibly form a black hole. These

However, it is not sufficient to rule out clusters of compact stellar remnants (eg, white dwarfs, neutron stars, or stellar black holes).

The third entry in Table 4 is based on infrared observations of stars that orbit an unseen mass in the center of the Milky Way. These observations by the Max Planck Institutue for Extraterrestrial Physics (eg, Gillessen et al. 2017) and the Univeristy of California, Los Angeles (eg, Boehle et al. 2016) groups require a central mass of $4 \times 10^6 M_\odot$ within a radius of 100 AU. One star (S2; S02) has been seen to complete nearly two elliptical orbits and multiple stars have traced partial orbits. All stars show a common gravitational focal position, which coincides with the radio source Sgr A* to within ≈ 0.001 arcseconds (Menten et al. 1997; Reid et al. 2007), and require the same central mass. The inferred mass density of $> 8 \times 10^{15} M_\odot \text{ pc}^{-3}$ is high enough to rule out very long-lived clusters of stars, as well as a speculative proposal of a central “ball” of heavy fermions (Munyanenza & Viollier 2002).

The fourth entry in Table 4 refers to the VLBI observations of the proper motion of Sgr A* reported in this paper. As shown in Section 3, Sgr A* *appears* to move along the plane of the Milky Way in a manner that can be completely accounted for by our orbit about the center of the Milky Way. This provides an upper limit of $\sim 1 \text{ km s}^{-1}$ for the intrinsic motion of Sgr A* itself. Stars near Sgr A* have been observed to move at thousands of km s^{-1} , and the only way that Sgr A* can be motionless is for it to be extremely massive. Both theory and direct simulations of the gravitational “Brownian” motion of a supermassive object at the center of the observed stellar cluster require Sgr A* to be in near thermal equilibrium with the stars within its sphere of influence. Our detailed simulations of the effects of the central stellar cluster on the expected motion of Sgr A*, described in Section 3, constrain its mass to likely exceed $1 \times 10^6 M_\odot$. A long history of VLBI observations have gradually improved measurements of the intrinsic size of Sgr A*; the most recent show Sgr A*’s emission has a radial extent of $\approx 0.18 \text{ AU}$ (Doeleman et al. 2008)⁵, which is comparable to the Schwarzschild radius for a $4 \times 10^6 M_\odot$ black hole.

Combining the lower limit for Sgr A*’s mass (from its lack of motion) with the size of

observations rule out long-lived clusters of normal stars as providing the central gravitational mass (Maoz 1998). However, this conclusion is based on the assumption of an *isolated* stellar cluster. The possibility of a quasi-steady-state condition, wherein stars beyond the 0.1 pc radius are gravitationally perturbed and enter the central region, replenishing those expelled, has yet to be considered in detail.

⁵The measured apparent size of Sgr A* is slightly smaller than that given by $3R_{Sch}$. This is as expected for the radiation from material in a disk orbiting the black hole at $3R_{Sch}$. Since the approaching material on one side is moving toward us at nearly the speed of light, this emission is boosted by relativistic aberration and Doppler shifts, causing this side to dominate the emissions.

the source yields both linear and volume mass densities that are within a factor of about three of the General Relativity limit for a black hole. This provides overwhelming evidence for a supermassive black hole at the center of the Milky Way.

5. Conclusions

In summary, infrared observations of stars orbiting an unseen mass concentration provide extremely strong evidence for a supermassive black hole at the center of the Milky Way. Radio observations associate that unseen mass with the radiative source Sgr A*, and its lack of motion requires a huge mass to reside within a region of a few Schwarzschild radii. If, following the infrared observations, there was any doubt that Sgr A* is a supermassive black hole, the radio observations should remove that doubt.

Facilities: VLBA

REFERENCES

- Boehle, A., Ghez, A. M., Schödel, R. et al. 2016, *ApJ*, 830, 17
- Chatterjee, P., Hernquist, L., & Loeb, A. 2002, *ApJ*, 572, 371
- Do, T., Hees, A., Ghez, A. et al. 2019, *Science*, 365, 664
- Doeleman, S. S., Weintraub, J., Rogers, A. E. e. et al. 2008, *Nature*, 455, 78
- Dorband, E. N., Hemsendorf, M. & Merritt, D. 2003, *J. Comp. Phys.*, 185, 484
- Figer, D. F., Kim, S. S., Morris, M., Serabyn, E., Rich, R. M., & McLean, I. S. 1999, *ApJ*, 525, 750
- Freitag, M., Amaro-Seoane, P. & Kalogera, V. 2006, *ApJ*, 649, 91
- Ghez, A. M., Salim, S., Hornstein, S. D et al. 2005, *ApJ*, 620, 744
- Ghez, A. M., Salim, S., Weinberg, N. N., Lu, J. R., Do, T., et al. 2008, *ApJ*, 689, 1044
- Gillessen, S., Plewa, P. M., Eisenhauer, F., Sari, R., Waisberg, I., et al. 2017, *ApJ*, 837, 30
- Gould, A. & Ramírez, S. V. 1998, *ApJ*, 497, 713
- Gravity Collaboration, Abuter, R. Amorim, A., Bauböck, M. et al. 2019, *A&A*, 625, 10

- Genzel, R., Eisenhauer, F. & Gillessen, S. 2010, *Rev. Mod. Phys.*, 82, 3121
- Maoz, E. 1998, *ApJ*, 494, L181
- Menten, K. M., Reid, M. J., Eckart, A. & Genzel, R. 1997, *ApJ*, 475, L111
- Merritt, D., Berczik, P. & Laun,, F. 2007, *ApJ*, 133, 533
- Munyanenza, F. & Viollier, R. D. 2002, *ApJ*, 564, 274
- Naoz, S., Will, C. M., Ramirez-Ruiz, E. et al. 2019, arXiv:1912:04910v1
- Reid, M. J., Readhead, A. C. S., Vermeulen, R. C., & Treuhaft, R. N. 1999, *ApJ*, 524, 816
- Reid, M. J., Menten, K. M., Genzel, R., Ott, T., Schödel, R., & Eckart, A. 2003, *ApJ*, 587, 208
- Reid, M. J., Menten, K. M., Trippe, S., Ott, T. & Genzel, R. 2007, *ApJ*, 659,, 378
- Reid, M. J. & Brunthaler, A. 2004, *ApJ*, 616, 872
- Reid, M. J. 2019, *IJMP-D*, 18, 889
- Reid, M. J., Menten, K. M., Brunthaler, A. et al. 2019, *ApJ*, 885,131
- Rogers, A. E. E. et al. 1994, *ApJ*, 434, L59
- Schödel, R. et al. 2002, *Nature*, 419, 694
- Stolte, A., Grebel, E. K., Brandner, W., & Figer, D. F. 2002, *A&A*, 394, 459

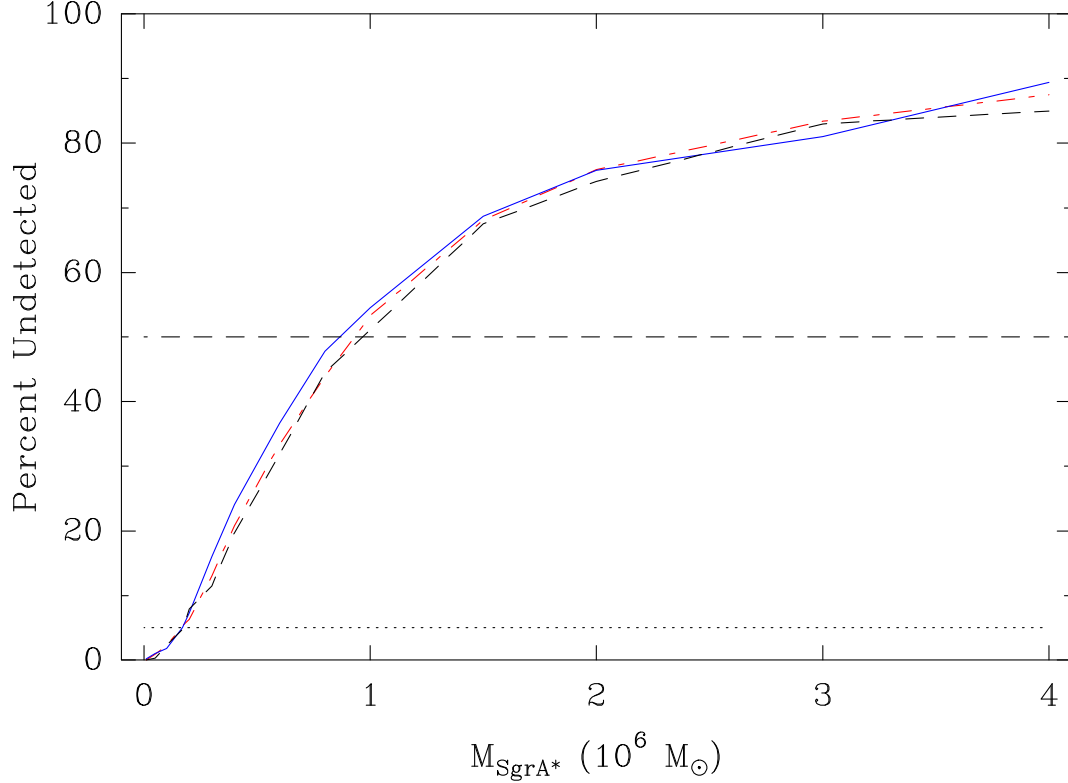


Fig. 4.— Results of simulations of the motion of Sgr A*, owing to random perturbations from the central stellar cluster, compared to observed limits. Plotted are the percentages of simulations that fall below the observed limits as a function of the assumed mass of Sgr A*. All simulations assume a stellar mass function index flatter by 0.5 compared to a standard Salpeter IMF. The blue solid line is our fiducial result, which uses the updated stellar distributions from Genzel, Eisenhauer & Gillessen (2010) with stellar density $\rho_*(R) = 1.35 \times 10^6 (R/R_b)^{-\gamma}$, where $R_b = 0.25$ pc is a break radius and γ is 1.3 for $R < R_b$ and 1.8 for larger radii. The black dashed line adds $\approx 4,000$ stellar-mass black holes with a Bahcall-Wolff cusp-like radial distribution with index $-7/4$ in the inner 0.2 pc. For comparison, the red dot-dashed line uses the stellar distribution from Paper II. Dotted and dashed lines indicate 5% and 50% of simulations that would not have been detected, corresponding to Sgr A* masses of about 0.2 and $1.0 \times 10^6 M_\odot$, respectively.

Table 1. Residual Position Offsets Relative to Sgr A*

Source	Date of Observation	East Offset (mas)	North Offset (mas)	ℓ^{II} Offset (mas)	b^{II} Offset (mas)
J1745–283	1995.178	-2.50 ± 0.5	-4.87 ± 0.8	-5.46 ± 0.73	-0.40 ± 0.60
	1996.221	0.37 ± 0.1	-0.25 ± 0.4	-0.02 ± 0.34	-0.44 ± 0.22
	1996.252	0.52 ± 0.1	0.59 ± 0.4	0.77 ± 0.34	-0.14 ± 0.22
	1997.211	3.67 ± 0.1	5.13 ± 0.4	6.29 ± 0.34	-0.46 ± 0.22
	1997.241	3.87 ± 0.1	5.08 ± 0.4	6.35 ± 0.34	-0.66 ± 0.22
	1997.241	3.76 ± 0.2	5.13 ± 0.6	6.33 ± 0.52	-0.54 ± 0.36
	1998.202	5.95 ± 0.2	10.58 ± 0.6	12.13 ± 0.52	0.43 ± 0.36
	1998.219	6.29 ± 0.2	10.42 ± 0.6	12.17 ± 0.52	0.06 ± 0.36
	1998.230	6.59 ± 0.2	11.34 ± 0.6	13.11 ± 0.52	0.28 ± 0.36
	1999.791	11.55 ± 0.2	18.95 ± 0.6	22.19 ± 0.52	0.01 ± 0.36
	1999.799	12.29 ± 0.2	20.40 ± 0.6	23.82 ± 0.52	0.13 ± 0.36
	1999.805	11.97 ± 0.2	19.75 ± 0.6	23.10 ± 0.52	0.07 ± 0.36
	2000.232	13.04 ± 0.2	22.60 ± 0.6	26.08 ± 0.52	0.64 ± 0.36
	2000.238	12.82 ± 0.2	22.49 ± 0.6	25.88 ± 0.52	0.77 ± 0.36
	2003.264	22.51 ± 0.1	38.94 ± 0.2	44.96 ± 0.18	1.08 ± 0.14
	2003.318	22.84 ± 0.1	39.18 ± 0.2	45.34 ± 0.18	0.92 ± 0.14
	2003.339	22.54 ± 0.4	39.59 ± 0.4	45.53 ± 0.40	1.38 ± 0.40
	2003.353	23.06 ± 0.1	39.41 ± 0.2	45.66 ± 0.18	0.85 ± 0.14
	2007.253	35.13 ± 0.2	61.29 ± 0.4	70.62 ± 0.36	1.95 ± 0.27
	2007.264	35.08 ± 0.1	61.06 ± 0.2	70.39 ± 0.18	1.87 ± 0.14
	2007.280	35.00 ± 0.1	61.66 ± 0.2	70.86 ± 0.18	2.25 ± 0.14
	2013.119	53.75 ± 0.1	94.01 ± 0.2	108.24 ± 0.18	3.11 ± 0.14
	2013.146	53.77 ± 0.1	94.25 ± 0.2	108.46 ± 0.18	3.22 ± 0.14
J1748–291	1996.221	1.04 ± 0.2	-2.09 ± 0.6	-1.24 ± 0.52	-1.98 ± 0.36
	1996.252	1.06 ± 0.2	-2.18 ± 0.6	-1.31 ± 0.52	-2.04 ± 0.36
	1997.211	4.53 ± 0.2	2.76 ± 0.6	4.72 ± 0.52	-2.43 ± 0.36
	1997.241	4.62 ± 0.2	2.44 ± 0.6	4.49 ± 0.52	-2.68 ± 0.36
	1998.202	7.65 ± 0.2	8.34 ± 0.6	11.10 ± 0.52	-2.19 ± 0.36
	1998.230	7.65 ± 0.2	8.10 ± 0.6	10.90 ± 0.52	-2.31 ± 0.36
	1999.791	12.87 ± 0.2	17.79 ± 0.6	21.89 ± 0.52	-1.72 ± 0.36
	1999.799	12.64 ± 0.2	17.18 ± 0.6	21.25 ± 0.52	-1.84 ± 0.36

Table 1—Continued

Source	Date of Observation	East Offset (mas)	North Offset (mas)	ℓ^{II} Offset (mas)	b^{II} Offset (mas)
	1999.805	12.94 \pm 0.2	17.84 \pm 0.6	21.97 \pm 0.52	−1.76 \pm 0.36
	2000.232	13.98 \pm 0.2	20.05 \pm 0.6	24.40 \pm 0.52	−1.48 \pm 0.36
	2000.238	14.13 \pm 0.2	20.54 \pm 0.6	24.90 \pm 0.52	−1.36 \pm 0.36
	2000.246	13.95 \pm 0.2	19.90 \pm 0.6	24.25 \pm 0.52	−1.54 \pm 0.36
	2003.264	23.42 \pm 0.2	37.89 \pm 0.6	44.54 \pm 0.52	−0.25 \pm 0.36
	2003.318	23.96 \pm 0.2	37.17 \pm 0.6	44.20 \pm 0.52	−1.09 \pm 0.36
	2007.253	36.16 \pm 0.2	59.41 \pm 0.6	69.55 \pm 0.52	+0.09 \pm 0.36
	2007.264	36.40 \pm 0.2	59.60 \pm 0.6	69.84 \pm 0.52	−0.02 \pm 0.36
	2007.280	36.42 \pm 0.2	59.58 \pm 0.6	69.83 \pm 0.52	−0.05 \pm 0.36
	2013.119	54.71 \pm 0.2	91.93 \pm 0.6	106.96 \pm 0.52	+1.20 \pm 0.36
	2013.146	54.82 \pm 0.2	92.04 \pm 0.6	107.12 \pm 0.52	+1.17 \pm 0.36

Note. — Position offsets are relative to Sgr A*, after removing the ≈ 0.7 degree differences of the background sources. The coordinate offsets are relative to the following J2000 positions: Sgr A* (17 45 40.0409, −29 00 28.118), J1745–283 (17 45 52.4968, −28 20 26.294), and J1748–291 (17 48 45.6860, −29 07 39.404). The conversion to Galactic coordinates is discussed in the Appendix of Reid & Brunthaler (2004), and their uncertainties have been updated to include the synthesized beam position angle in the propagation of errors. The positions for epochs before 1998 have been corrected for the second-order effects of processing the phase-reference data from Sgr A* with J2000 coordinates of (17 45 40.0500, −29 00 28.120).

Table 2. Apparent Relative Motions

Source – Reference	Easterly Motion (mas y ⁻¹)	Northerly Motion (mas y ⁻¹)	ℓ^{II} Motion (mas y ⁻¹)	b^{II} Motion (mas y ⁻¹)
Sgr A* – J1745–2820	-3.147 ± 0.008	-5.578 ± 0.011	-6.402 ± 0.010	-0.219 ± 0.008
Sgr A* – J1748–2907	-3.166 ± 0.008	-5.606 ± 0.019	-6.434 ± 0.016	-0.218 ± 0.013
Sgr A* – Combined	-3.156 ± 0.006	-5.585 ± 0.010	-6.411 ± 0.008	-0.219 ± 0.007

Note. — Motions values are from weighted least-squares fits to the data in Table 1, with uncertainties scaled to give a reduced chi-squared of unity. Equatorial motions are in the J2000 system and Galactic motions are based on Galactic coordinates transformed to J2000 as described in the appendix of Reid & Brunthaler (2004). “Combined” motions are variance weighted averages of the individual results.

Table 3. Estimating Sgr A*’s Intrinsic Motion

Description	μ_l (mas yr ⁻¹)	μ_b (mas yr ⁻¹)
Sgr A*’s <i>apparent</i> motion ^a	-6.411 ± 0.008	-0.219 ± 0.007
Reflex of Sun’s Galactic orbit ^b	-6.396 ± 0.057	-0.197 ± 0.018
Difference: Sgr A*’s <i>intrinsic</i> motion	-0.015 ± 0.058	-0.022 ± 0.019
	(km s ⁻¹)	(km s ⁻¹)
Difference: assuming $R_0 = 8.15$ kpc	-0.58 ± 2.23	-0.85 ± 0.75

^aProper motion Galactic longitude (μ_l) and latitude (μ_b) from Table 2.

^bAdopting the Galactic orbital values of the Sun from parallaxes and proper motions of masers associated with massive young stars by Reid et al. (2019). Longitudinal motion: $(\Theta_0 + V_\odot)/R_0 = 30.32 \pm 0.27$ km s⁻¹ kpc⁻¹. Latitudinal motion: $W_\odot = 7.6 \pm 0.7$ km s⁻¹.

Table 4. Density Limits for SMBH Candidates

Object	Mass (M_{\odot})	Radius (AU)	M/R (kg/m)	Density ($M_{\odot} \text{ pc}^{-3}$)
Globular Cluster	1×10^6	2×10^5	7×10^{19}	3×10^5
NGC 4258	4×10^7	$< 2 \times 10^4$	$> 3 \times 10^{22}$	$> 1 \times 10^{10}$
Stellar orbits	4×10^6	< 100	$> 5 \times 10^{23}$	$> 8 \times 10^{15}$
Sgr A* motion	$> 1 \times 10^6$	0.18	$> 7 \times 10^{25}$	$> 4 \times 10^{23}$
SMBH ($3R_{Sch}$)	4×10^6	0.24	2×10^{26}	6×10^{23}

Note. — The columns under the headings M/R and Density give the critical “linear” and volume densities, appropriate for $R_{crit} = 3R_{Sch}$ as discussed in Section 4.